Patrick Akata Nwofe\* and Mutsumi Sugiyama

# Influence of deposition time and annealing treatments on the properties of chemically deposited Sn<sub>2</sub>Sb<sub>2</sub>S<sub>5</sub> thin films and photovoltaic behavior of Sn<sub>2</sub>Sb<sub>2</sub>S<sub>5</sub>-based solar cells

https://doi.org/10.1515/zna-2020-0166 Received June 20, 2020; accepted July 28, 2020; published online September 11, 2020

**Abstract:** Thin films of chemical bath deposited tin antimony sulphide (Sn<sub>2</sub>Sb<sub>2</sub>S<sub>5</sub>) were tuned by varying the deposition time between 1 and 3 h, and postdeposition heat treatments. The films were grown on soda lime glass (SLG) and on molybdenum glass (Mo-SLG) substrates, respectively. The film thickness increased with deposition time up to 2 h and decreased thereafter. Structural analysis from X-ray diffractometry showed that the films were single phase. This was corroborated by X-ray photoelectron spectroscopy (XPS) analysis. Energy-dispersive spectroscopy results give antimony/sulphur (Sb/S) ratio and antimony/tin (Sb/Sn) ratio that increased with deposition time in the SLG substrates only. Optical constants extracted from optical spectroscopy measurements give optical absorption coefficient ( $\alpha$ ) > 10<sup>4</sup> cm<sup>-1</sup>, and direct energy bandgap with values in the range 1.30 to 1.48 eV. The Hall effect measurements performed on films grown on the SLG substrates indicated that the films were p-type electrical conductivity with electrical resistivity in the range 10<sup>3</sup> to  $10^4$   $\Omega$ cm. The films grown on the Mo-SLG served as absorber layers to fabricate thin film heterojunction solar cell devices in the substrate configuration with a cadmium sulphide (CdS) window partner. The best device yielded a short-circuit current density of 20 mA/cm<sup>2</sup>, open-circuit voltage of 0.012 V and a solar conversion efficiency of 0.04%.

**Keywords:** absorber layers; chemical bath deposition; deposition time; Sn<sub>2</sub>Sb<sub>2</sub>S<sub>5</sub>; solar conversion efficiency.

#### 1 Introduction

Thin film solar cells have been established over the years as one of the most viable options in photovoltaic technology. However the cost per unit watts of solar cells is still very high hence the universal struggle by various research groups in probing the potentials of different inorganic materials for photovoltaic applications still persists. Such inorganic materials must satisfy certain criteria including abundance of the constituent elements, environmentally acceptable, lowcost, high optical absorption coefficient, direct energy bandgap, and p-conductivity type amongst others. Sn<sub>2</sub>Sb<sub>2</sub>S<sub>5</sub> thin films are known to satisfy these requirements based on current literature reports [1-19], added with the flexibility in device designs as Sn<sub>2</sub>Sb<sub>2</sub>S<sub>5</sub> thin films can be prepared using different deposition techniques including Bridgman method [1–4], photothermal deflection spectroscopy [5], thermal evaporation [6–17], electropyroelectric technique [18], and Rf-sputtering techniques [19]. Sn<sub>2</sub>Sb<sub>2</sub>S<sub>5</sub> belongs to the  $(SnS)_x(Sb_2S_3)_y$   $(1 \le x \le 5, 1 \le y \le 3)$  sulfosats family. Other phases of tin antimony sulphide of the form; (SnS)<sub>x</sub>(Sb<sub>2</sub>S<sub>3</sub>)<sub>y</sub>  $(1 \le x \le 5, 1 \le y \le 3)$  based thin films have been prepared using thermal evaporation [20–47], oblique angle deposition [48], chemical bath deposition (CBD) [49-54], electrodeposition [55–56], and recently by spin coating [57]. Different phases of tin antimony sulphide thin films of the form (SnS)<sub>x</sub>(Sb<sub>2</sub>S<sub>3</sub>)<sub>v</sub>  $(1 \le x \le 5, 1 \le y \le 3)$  includes;  $SnSb_2S_4$  [20–29, 40],  $Sb_2Sn_5S_9$  [13, 58], SnSb<sub>4</sub>S<sub>7</sub> [30–34], Sn<sub>4</sub>Sb<sub>6</sub>S<sub>13</sub> [37–39, 59], Sn<sub>3</sub>Sb<sub>2</sub>S<sub>6</sub> [40–42, 48, 60–61], Sn<sub>6</sub>Sb<sub>10</sub>S<sub>21</sub> [44, 62], Sn<sub>6</sub>Sb<sub>2</sub>S<sub>11</sub> [50], and Sn<sub>6</sub>Sb<sub>17</sub>S<sub>29</sub> [50]. It is pertinent to note that research reports in all these phases are still very few compared to that of other sulfosats including SnS thin films. The materials, optical and electrical properties of the  $(SnS)_x(Sb_2S_3)_y$   $(1 \le x \le 5, 1 \le y \le 3)$  thin films have been accessed by different research groups [8, 10, 12, 19, 23, 36, 49–51, 54], and all points to the suitability of the films as absorber layers in heterojunction thin film solar cell devices. Analytical reports using suitable software to probe the

<sup>\*</sup>Corresponding author: Patrick Akata Nwofe, Department of Electrical Engineering, Faculty of Science and Technology, Tokyo University of Science, 20641 Yamazaki, Noda, 278-8510, Japan; and Department of Industrial Physics, Faculty of Science, Ebonyi State University, P.M.B 051, Abakaliki, Nigeria, E-mail: patricknwofe@gmail.com

Mutsumi Sugiyama, Department of Electrical Engineering, Faculty of Science and Technology, Tokyo University of Science, 20641

Yamazaki, Noda 278-8510, Japan, E-mail: mutsumi@rs.tus.ac.jp

potentials of  $(SnS)_x(Sb_2S_3)_y$  ( $1 \le x \le 5$ ,  $1 \le y \le 3$ ) thin films to date is only contained in the work of Gassoumi et al. [63] using the Modified Becke-Johnson potentials. However extensive research work is still needed to unravel the potentials of these phases as only few reports are available on the photovoltaic performance of  $(SnS)_x(Sb_2S_3)_y$   $(1 \le x \le 5, 1 \le y \le 3)$ -based solar cells [49, 51, 54]. Additionally, good absorber layer requirements also include low electrical resistivity and good crystallinity. Sn<sub>2</sub>Sb<sub>2</sub>S<sub>5</sub> thin films is relatively novel hence there are limited reports on the materials, electrical and device properties in the literature. Different authors [10, 20] have reported electrical resistivities of  $(SnS)_x(Sb_2S_3)_y$   $(1 \le x \le 5,$  $1 \le y \le 3$ ) thin films to be in the range obtained in the more advanced thin film solar cells such as copper indium gallium diselenide- and cadmium telluride-based devices. Tin antimony sulphide thin films are known to exhibit bipolar electrical conductivity according to the literature [10, 16, 35-36, 51, 53]. In our recent report [53], emphasis was on the influence of varying tin amount on the materials, optical, and electrical properties of tin antimony sulphide thin films at fixed deposition time. The present investigation centred on the effect of different deposition time on the properties of the films and the feasibility of using Sn<sub>2</sub>Sb<sub>2</sub>S<sub>5</sub> thin films produced using low-cost deposition technique as possible absorber layers in thin film heterojunction solar cell devices as a pioneering report. The photovoltaic parameters are comparable to the report of other authors in SnSb<sub>2</sub>S<sub>4</sub>, Sn<sub>6</sub>Sb<sub>10</sub>S<sub>21</sub>, and Sn<sub>3</sub>Sb<sub>2</sub>S<sub>6</sub> related thin film heterojunction solar cells [49, 51, 54], respectively. The current report gives a comprehensive information on the status of  $(SnS)_x(Sb_2S_3)_y$   $(1 \le x \le 5, 1 \le y \le 3)$ thin films and also opened a new pathway in Sn<sub>2</sub>Sb<sub>2</sub>S<sub>5</sub> absorber layers for photovoltaic applications and will improve significantly over time.

#### 2 Experimental details

### 2.1 General steps and preparation of absorber layers

One of the fundamental steps in thin film preparation is substrate cleaning. This was done in an ultrasonic bath with 2-propanol and ultrapure distilled water and finally stored in a vacuum environment. The source materials used to grow the absorber layers included antimony trichloride (SbCl<sub>3</sub>) as source of antimony ions (Sb<sup>3+</sup>), tin (II) chloride dihydrate (SnCl<sub>2</sub>.2H<sub>2</sub>O) as source of (Sn<sup>2+</sup>) ions, anhydrous sodium thiosulphate (Na<sub>2</sub>S<sub>2</sub>O<sub>3</sub>) as source of sulphur ions (S<sup>2-</sup>), tartaric acid (C<sub>4</sub>H<sub>6</sub>O<sub>6</sub>) as complexing

agent, and acetone (CH<sub>3</sub>COCH<sub>3</sub>). The source materials for the window layers are as follows: cadmium sulphate  $(CdSO_4)$  as source of  $Cd^{2+}$  ions, thiourea  $(SC(NH_2)_2)$  as source of  $S^{2-}$  ions, and ammonia (NH<sub>3</sub>) to regulate the pH. Ultrapure distilled water was used in all the chemical preparations, and all the source materials were procured from FUJIFILM Wako Pure Chemical Corporation, Japan. The details of further preparation steps are given in our previous report [53]. According to the literature, the family of tin antimony sulphide ternary compounds of the form  $Sb_2S_3.nSnS$  for n = 1, 2, and 3 was synthesized by Wang and Eppelsheimer [64] and the authors observed structural series for the Sn<sub>2</sub>Sb<sub>2</sub>S<sub>5</sub> phase. It is a common knowledge that CBD do occur by different mechanisms through one or combinations of (i) simple cluster (ii) complex-cluster (iii) complex-complex (iv) complex-ion (v) ion-ion, and (vi) simple-ion process. Whichever is the reaction pathway, the supersaturation condition must be satisfied. This implies that the ionic product (Qip) must be greater than the solubility product  $(K_{sp})$ ,  $(Q_{ip} > K_{sp} = super$ saturation). Additionally, complexing agents act to reduce spontaneous precipitation and hence slow down reaction rates. In the bath containing the Sn<sup>2+</sup>, Sb<sup>3+</sup>, and S<sup>2-</sup> ions, respectively, the following reactions are expected to occur:

$$2SnCl_2.2H_2O + 2C_4H_6O_6 \Leftrightarrow 2[Sn(C_4H_6O_6)]^{2+} + 4Cl^{-} + 4H_2O$$
(1)

$$2[Sn(C_4H_6O_6)]^{2+} + 2S^{2-} \rightarrow 2SnS + 2C_4H_6O_6$$
 (2)

$$2Sb^{3+} + 3S_2O_3^{2-} \rightarrow Sb_2(S_2O_3)_3$$
 (3)

$$S_2O_3^{2-} + H^+ \to S + HSO_3^-$$
 (4)

$$S + 2e^- \rightarrow S^{2-} \tag{5}$$

$$2Sb^{3+} + 3S^{2-} \to Sb_2S_3 \tag{6}$$

$$2SnS + Sb_2S_3 \rightarrow Sn_2Sb_2S_5 \tag{7}$$

The free radicals of the  $\rm Sn^{2+}$  ions indicated in Equation (1) are regulated by the presence of the tartaric acid. In the presence of metallic ion, thiosulphate are known to form complex as given in Equation (3) according to the literature [65]. The  $\rm Sn^{2+}$  ions reacts with  $\rm S^{2-}$  ions released from the hydrolytic decomposition of the thiosulphate ions as given in Equations (4) and (5), respectively. The formation of the  $\rm Sn_2Sb_2S_5$  thin film is based on the reaction from Equations (2) and (6).

## 2.2 Preparation of window layers and fabrication of Sn<sub>2</sub>Sb<sub>2</sub>S<sub>5</sub>-related thin film solar cells

To prepare the CdS layer; a 0.154~g of CdSO $_4$  was included in a precleaned beaker containing 25 ml of water, a 2.854~g of SC(NH $_2$ ) $_2$  in a precleaned beaker with 50 ml of water and stirring done for 15 min in each case. In a separate beaker containing 366 ml of water, a 65 ml of NH $_3$  was added and stirred. The Cd $^{2+}$  source was then added, followed by the S $^{2-}$  source with continuous stirring. The substrates were then inserted when the bath temperature was 65 °C and deposition rate was maintained at 6.25~nm/min.

The  $Sn_2Sb_2S_5$ -based solar devices were fabricated using the substrate configuration in the form: glass/Mo/ $Sn_2Sb_2S_5$ /CdS/i-ZnO/Al:ZnO/Ni/Al. The deposition technique for each layer includes the following;  $Sn_2Sb_2S_5$  absorber and CdS buffer by CBD, an i-ZnO/Al:ZnO transparent conducting oxide by RF-sputtering, and Ni/Al grid contacts by electron beam evaporation. The cell area was 0.13 cm².

#### 2.3 Characterisation

The effect of the different deposition times on the physical properties of the  $Sn_2Sb_2S_5$  layers grown on both substrates were systematically analysed using suitable characterization tools. A Rigaku Ultima (IV) X-ray diffraction equipment with a CuK $\alpha$  radiation, operated in the  $\theta{-}2\theta$  scan mode in 0.02 intervals at a scan range of 10–70 degrees was used to investigate the crystal structure and phase present in the films. The Hitachi S-4800 scanning electron

microscope operated at a voltage of 5 kV and current of 7.6  $\mu$ A was used to study the surface morphology. Energy-dispersive spectroscopy (EDS) (Hitachi Miniscope TM-1000) and JEOL JPS-9000MC X-ray photoelectron spectroscopy (XPS) were used for the compositional analysis and chemical states. Optical spectroscopy was done with U-4100 Hitachi Spectrophotometer at a wavelength range of 300–1500 nm, and the optical constants extracted using basic equations from the literature. Hall effect equipment attached with the ResiTest 8300 model was used for electrical characterisation. The J–V curves (Keithley 2400) were obtained under illumination with a light source of 100 mW/cm² at AM 1.5 standard conditions.

#### 3 Results and discussion

#### 3.1 Structural analysis

Figure 1 show X-ray diffractograms of  $Sn_2Sb_2S_5$  films grown on soda lime glass (SLG) substrates while Figure 2 is for molybdenum (Mo)-SLG substrates. The plots indicated that the films were all polycrystalline irrespective of the substrates at the different deposition times. The films crystallized in the orthorhombic crystal structure corresponding to the Joint Committee on Powder and Diffraction Standards (JCPDSs) No. 00-044-0829 [66]. The films exhibited relatively constant diffraction peaks for films grown at  $\leq 2$  h and increased thereafter independent of the substrates. The increased texturing observed at the longer deposition time was due to the effect of dissociation arising from the complex-ion interaction and/or ion-ion interaction during the film growth. Another clear possibility is that of the

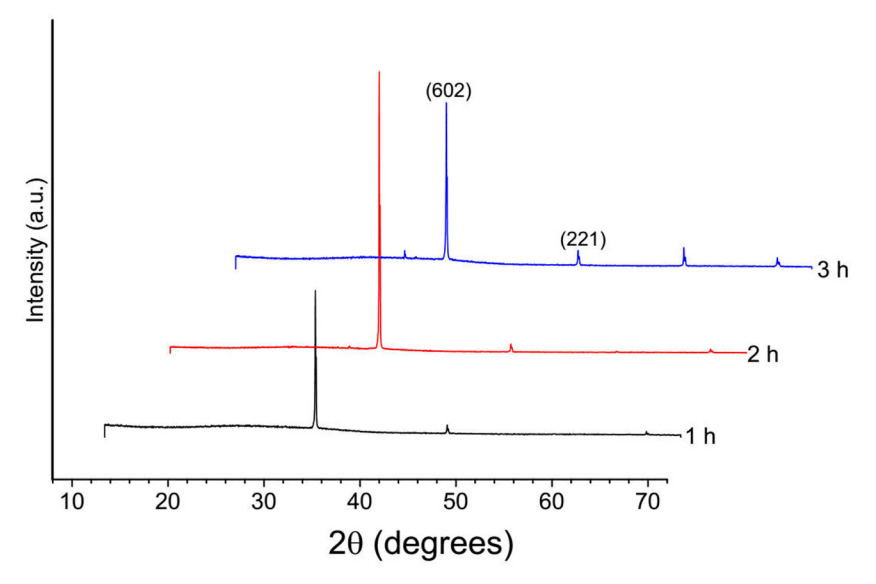


**Figure 1:** X-ray patterns of Sn<sub>2</sub>Sb<sub>2</sub>S<sub>5</sub> thin films on soda lime glass (SLG) substrates at different deposition times.

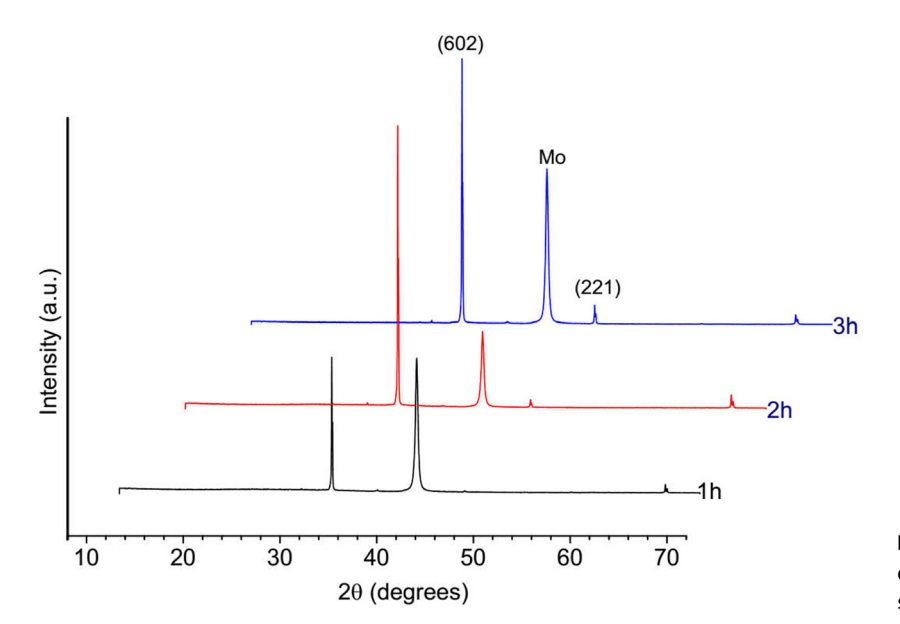


Figure 2: X-ray patterns of  $Sn_2Sb_2S_5$  thin films on molybdenum soda lime glass (Mo-SLG) substrates at varying deposition times.

migration of ions of Sn<sup>2+</sup> oxidation states to Sn<sup>5+</sup> states in the deposition matrix during the film formation. The increased texturing was more pronounced for films grown with the SLG substrates compared to that of the Mo-SLG substrates. This was attributed to the difference in the hydrophobicity and surface energies of the different substrates. The films grown in the former show preferential plane at  $2\theta \approx 31.77$ , while the preferential plane occurred at  $2\theta \approx 31.93$  and at 40.72 in the latter. The diffraction peak at  $2\theta \approx 40.72$  was attributed to Mo peak. Independent of the different substrates, other clear defined diffraction peaks occurred at  $2\theta \approx 45.65$ , 56.68, and 66.42 especially at the higher deposition time. The most prominent Bragg peaks observed at  $2\theta \approx 31.77$  in the former and at  $2\theta \approx 31.93$  in the latter were assigned to the (602) reflections of the Sn<sub>2</sub>Sb<sub>2</sub>S<sub>5</sub> phase in line with the literature [4, 7, 66]. The diffraction peaks observed in this study is in agreement with the report of other authors in Sn<sub>2</sub>Sb<sub>2</sub>S<sub>5</sub> thin films grown by different technique [4, 7, 14]. Additionally, the literature of preferential peaks for Sn<sub>2</sub>Sb<sub>2</sub>S<sub>5</sub> thin films indicates that the (602) peaks are more commonly observed as shown in Table 1. The consistent pattern in the diffraction planes as indicated in Figures 1 and 2 is a clear indication that the films crystallized in a single-phase structure. The intensity of the diffraction peak of the preferential plane increased up to a deposition time of 2 h and decreased thereafter for films grown on SLG substrates. This behaviour was attributed to the effect of dissociation as indicated earlier. Data obtained from X-ray diffractometry (XRD) measurements were used to deduce relevant structural parameters including interplanar spacing  $(d_{hkl})$ , lattice constants (a, b, c), crystallite size, microstrain, dislocation density, and number of

crystallites. In particular, the crystallite sizes were calculated from the Scherrer's formula, the interplanar spacings from Bragg's diffraction equation and lattice constants using the formula for an orthorhombic system. Accordingly, the following equations were employed [1, 32, 38, 49, 66–67];

$$D = \frac{0.94\lambda}{\beta \cos \theta} \tag{8}$$

$$\frac{1}{d^2} = \frac{h^2}{a^2} + \frac{k^2}{b^2} + \frac{l^2}{c^2} \tag{9}$$

$$\zeta = \frac{\beta}{4\tan\theta} \tag{10}$$

$$\delta = \frac{1}{D^2} \tag{11}$$

$$N = \frac{t}{D^3} \tag{12}$$

As indicated in Equations (8)–(12), D is the crystallite size,  $\lambda$  is the wavelength of the X-ray (1.5410 Å), 0.94 is the Scherrer's constant,  $\theta$  is the diffraction angle,  $\beta$  is the full width at half maximum, d is value of d-spacing of lines in XRD pattern, (hkl) are miller indices,  $\zeta$  is the microstrain,  $\delta$  is the dislocation density, N is the number of crystallites, where t is the film thickness. Analysis done using Equation (9) indicates that the values of the lattice parameters for the  $Sn_2Sb_2S_5$  films are; a = 19.58 Å, b = 3.82 Å, and c = 11.51 Å. These values are in agreement with the JCPDS No. 00-044-0829 and with the reports of other authors in the literature [68]. Table 2 show the results obtained from the analysis using the corresponding equations for the XRD

Table 1: Library of selected crystallographic properties of Sn<sub>2</sub>Sb<sub>2</sub>S<sub>5</sub> thin films according to the literature.

References	Crystallographic properties							
	2θ (°)	Preferential plane (hkl)	PDF	Crystal structure				
[1]	Not given	104	01-078- 1468	Orthorhombic				
[2]	Not given	602	Not given	Monoclinic				
[3]	Not given	013	044- 0829	Not given				
[4]	31.67	602	Not given	Not given				
[6]	32	602	044- 0829	Orthorhombic				
[7]	Not given	602	044- 0829	Orthorhombic				
[10]	Not given	104	Not given	Not given				
[11]	31.79	104	01-078- 1468	Orthorhmbic				
[12]	Not given	211	Not given	Not given				
[14]	Not given	602	044- 0829	Not given				
[16]	Not given	402	Not given	Not given				
[17]	31.67	602	35-1469	Not given				
[18]	Not given	211	Not given	Not given				
[19]	Not given	311	Not given	Not given				

data from films grown on SLG substrates while Table 3 show for films grown on Mo-SLG substrates. It was observed that the crystallites size increased consistently in the SLG substrates for deposition time ≤2 h and exhibited a marginal decrease thereafter. The values of the crystallite sizes were relatively higher for films grown on Mo-SLG substrates compared to those grown on SLG substrates. This behaviour is not surprising as the different substrates contains different chemical bonding properties and surface effects. Variation of structural parameters associated with different deposition conditions, deposition techniques, and other related indices are commonly observed in thin films according to literature reports [20, 32–33, 39, 49, 54].

#### 3.2 Morphological analysis

The Scanning electron microscopy (SEM) micrographs for the Sn<sub>2</sub>Sb<sub>2</sub>S<sub>5</sub> thin films grown at different deposition time on different substrates are shown on Figure 3. The morphology of the films indicated a densely packed relatively rice-like morphology for films grown on the SLG substrates. The grain shapes observed for films grown on the Mo-SLG substrates differed completely as densely packed spherical-shaped grains were intertwined with the relatively rice-like grain shapes. The difference in the grain morphology was attributed to the effect of the different bonding properties of the substrates as indicated earlier. Additionally, the contributions of the different hydrophobicity and surface energies of the substrates are likely very paramount to the observed phenomena. Due to the novelty of Sn<sub>2</sub>Sb<sub>2</sub>S<sub>5</sub> thin films, there is currently no report on scanning electron microscopy studies as to compare the morphology of the films with the literature. However, Mami et al. [6] recently observed point-like grain morphology from optical microscopy techniques and attributed it to the migration of Sn<sup>2+</sup> oxidation states to Sn<sup>5+</sup> states induced by annealing treatments.

Table 2: Variation of structural indices of Sn<sub>2</sub>Sb<sub>2</sub>S<sub>5</sub> thin films grown on soda lime glass (SLG) substrates at different deposition times.

Deposition time (h)						Structural indices
	2θ (°)	β (°)	ζ	D (nm)	$oldsymbol{\delta}  imes \mathbf{10^{16}}$ (nm $^{-2}$ )	$ extit{N}  imes  extstyle 10^{15}  ext{ (nm}^{-2)}$
1	31.9325	0.0628	0.0252	13.60	5.41	0.99
	45.6701	0.0816	0.0199	12.70	6.20	1.22
av			0.0226	13.15	5.81	1.11
2	31.7744	0.0576	0.0233	14.8	4.57	0.87
	45.4897	0.101	0.0249	10.2	9.59	2.63
	66.2727	0.0924	0.0102	19.5	2.64	0.38
av			0.0194	14.8	5.60	1.29
3	31.9310	0.0677	0.0272	12.6	6.29	1.17
	45.6584	0.0870	0.0213	11.9	7.05	1.39
	56.6771	0.0792	0.0130	16.6	3.61	0.51
	66.4180	0.112	0.0122	16.2	3.81	0.55
av			0.0184	14.3	5.19	0.91

av refers to average values of the structural indices.

**Table 3:** Variation of structural indices of  $Sn_2Sb_2S_5$  thin films grown on molybdenum soda lime glass (Mo-SLG) substrates at different deposition times.

Deposition time (h)					Structura	al indices
	2θ (°)	β (°)	ζ	D (nm)	$\delta \times 10^{16}$ (nm <sup>-2</sup> )	N x 10 <sup>15</sup> (nm <sup>-2</sup> )
1	31.7565	0.0716	0.0289	11.9	7.07	8.32
	45.4750	0.0819	0.0201	12.6	6.29	6.70
	66.2592	0.0998	0.0110	18.0	3.08	2.40
av			0.0200	14.2	5.48	5.90
2	31.7439	0.0590	0.0238	14.4	4.80	8.64
	45.4221	0.0750	0.0082	24.1	1.72	1.85
av			0.0160	19.3	3.26	5.24
3	31.9302	0.0651	0.0261	13.1	5.08	5.95
	45.4945	0.0800	0.0197	12.9	5.99	6.22
	56.5474	0.0546	0.0090	24.1	1.73	0.961
	66.2626	0.0925	0.0102	19.5	2.64	1.82
av			0.0162	17.4	4.05	3.74

av refers to average values of the structural indices.

#### 3.3 Compositional analysis

#### 3.3.1 Energy-dispersive spectroscopy studies

Table 4 show the compositional properties of the Sn<sub>2</sub>Sb<sub>2</sub>S<sub>5</sub> films as observed from EDS analysis. The atomic percentages of antimony increased with an increase in the deposition time for films grown on the SLG substrates. The Sb/ Sn and Sb/S ratios also exhibited similar trend in the films grown on the SLG substrates. However for films grown on Mo-SLG substrates, the atomic percentages of antimony, Sb/Sn and Sb/S ratios all increased up to a deposition time of 2 h and decreased thereafter. A close look at Table 4 reveals that the atomic percentages of molybdenum were 72.2, 38.3, and 64.3% at the respective deposition times. These values exhibit similar trend with the variation of Mo peaks in Figure 2. The observed relative loss of stoichiometry of the Sn<sub>2</sub>Sb<sub>2</sub>S<sub>5</sub> atomic percentage composition (22:22:56) is attributed to (i) different molarities of the source materials used to form the ternary compound  $(Sn_2Sb_2S_5)$  thin films, (ii) inhomogeneity in the ion-ion interaction or complex-ion interaction during the deposition process. Deviations from stoichiometry of Sn<sub>2</sub>Sb<sub>2</sub>S<sub>5</sub> phase are commonly observed in the literature [12, 16, 19].

#### 3.3.2 X-ray photoelectron spectroscopy studies

The elemental composition and chemical states of the  $Sn_2Sb_2S_5$  thin films at the respective deposition conditions was adequately analysed by the XPS studies. Figure 4a

gives typical XPS plots in the binding energy range of 0 to 1000 eV for films grown at a deposition time of 2 h in both substrates while Figure 4b show the wide scan resolution plots for the  $Sn3d_{5/2}$ ,  $Sn3d_{3/2}$ ,  $Sb3d_{5/2}$ ,  $Sb3d_{3/2}$ , and  $S2p_{3/2}$  at the respective deposition times in both substrates. The measurements of the core-level spectra were performed after a soft surface etching process.

The presence of Sn, Sb, and S were clearly established as the spectrum (Figure 4a) showed several peaks related to Sn 4d, double Sn 3d, Sn 3p, Sn 3s, Sb 3d, S 2p, S 2s, C 1s, and O 1s. The peaks related to oxygen are either present due to contaminant picked up during film processing, postdeposition heat treatments or from local ambient while the peaks related to C was probably from the reference as the reflections in the XPS spectrum was calibrated by the XPS line of C 1s. The high-resolution scan of the Sn 3d doublet (Figure 4b) indicated the films were strongly influenced by the deposition conditions. For instance, the films grown on the SLG substrates at a deposition time of 1 h exhibited two peaks at binding energies of 485.5 and 494.2 eV, related to the Sn<sup>2+</sup> valence states that is associated to the Sn $3d_{5/2}$ and  $Sn3d_{3/2}$  energy levels of Sn atoms. This gives a peak splitting value of 8.7 eV. For deposition time of 2 h, the binding energies of the Sn3 $d_{5/2}$ and Sn3 $d_{3/2}$ energy levels occurred at 484.8 and 494 eV, respectively, and thus yielded binding energy difference of 9.2 eV. The increase in the deposition time to 3 h did not exhibit any difference with the binding energy values for films grown at 2 h. However the width of the Sn3 $d_{5/2}$  peak was slightly higher for films grown at deposition time of 3 h. For films grown on Mo-SLG substrates at deposition times between 1 and 3 h, the Sn 3d doublet occurred as follows: 485 and 494 eV, 485.1 and 494.6 eV, 485.4 and 495 eV corresponding to  $Sn3d_{5/2}$  and  $Sn3d_{3/2}$  for the respective deposition times. This gives a spin energy separation of 9.0 eV, 9.5 eV, and 9.6 eV, implying an increase with increase in the deposition time. The values of the binding energies are in agreement with the report of other authors [69]. The characteristic of antimony in the 3+ oxidation state are mostly reflected in two main peaks of the Sb 3d doublet and generally occur at binding energies from 530 to 537 eV for Sb3 $d_{5/2}$  and 528 to 539.5 eV for Sb3 $d_{3/2}$  [70-76]. The different deposition times also influenced the variation of the binding energies of the Sb 3d doublet significantly. In the SLG substrates, the Sb3 $d_{5/2}$  and Sb3 $d_{3/2}$  appeared at binding energy values of 529 and 539 eV for films grown for 1 h, and 528.5 and 538 eV for films grown at deposition times ≥2 h. This gives a decrease in the binding energy separation from 10.0 to 9.5 eV at the respective deposition times. For films grown on Mo-SLG substrates, the binding energies for Sb3 $d_{5/2}$  and Sb3 $d_{3/2}$  are located at 531 and 540 eV for films grown at 1 h,

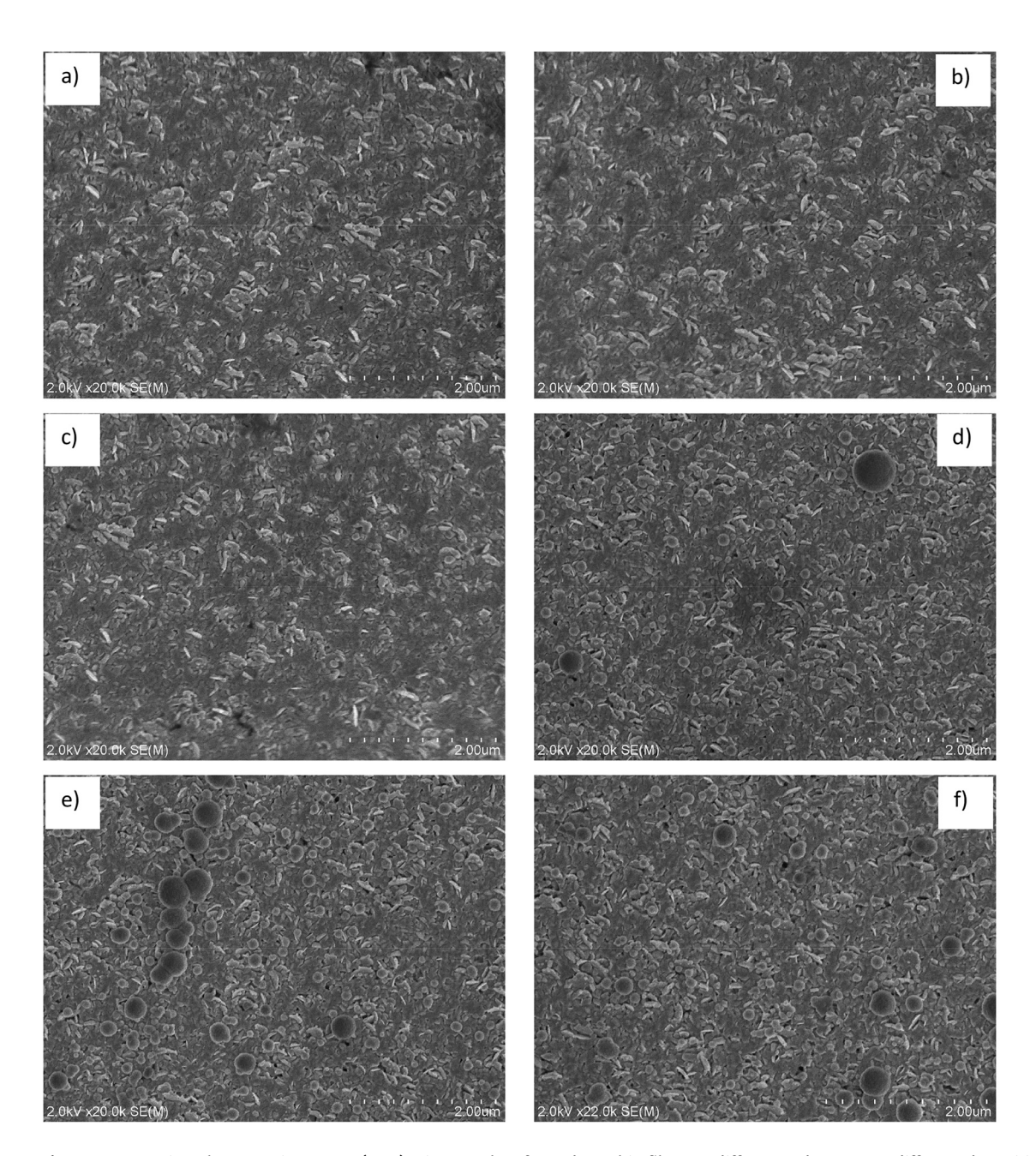
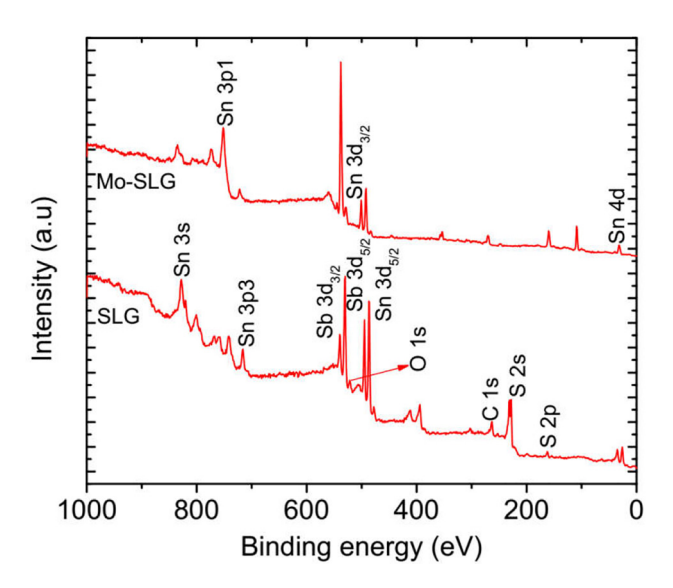


Figure 3: Scanning electron microscopy (SEM) micrographs of Sn<sub>2</sub>Sb<sub>2</sub>S<sub>5</sub> thin films on different substrates at different deposition times; (a) soda lime glass (SLG) at 1 h, (b) SLG at 2 h, (c) SLG at 3 h, (d) molybdenum (Mo)-SLG at 1 h, (e) Mo-SLG at 2 h, and (f) Mo-SLG at 3 h.

Table 4: Variation of film thickness and compositional properties of Sn<sub>2</sub>Sb<sub>2</sub>S<sub>5</sub> thin films on different substrates at different deposition times.

Dep. time (h)	t (µm)				А	tomic%	<i>t</i> (µm)					A	tomic%
						SLG						ı	Mo-SLG
		Sn	Sb	S	Sb/Sn	Sb/S	_	Sn	Sb	S	Мо	Sb/Sn	Sb/S
1	0.250	43.9	20.3	35.8	0.46	0.57	0.140	11.1	6.60	10.1	72.2	0.60	0.65
2	0.280	49.0	30.9	20.1	0.63	1.54	0.260	25.9	20.0	15.8	38.3	0.77	1.27
3	0.235	39.8	38.5	21.7	0.97	1.77	0.134	13.0	8.50	14.2	64.3	0.65	0.60

Mo-SLG, molybdenum soda lime glass.



**Figure 4a:** Typical full scan X-ray photoelectron spectroscopy (XPS) spectra of  $Sn_2Sb_2S_5$  thin films on different substrates at a deposition time of 2 h.

and at 529 and 538 eV for films grown at 2 h, respectively. This yielded a constant peak splitting of 9.0 eV. At a deposition time of 3 h, only the Sb3 $d_{5/2}$  singlet was observed at binding energy of 531.5 eV. The absence of the  $Sb3d_{3/2}$  was attributed to the effect of the substrate as indicated in sections Structural analysis and Morphological analysis, respectively. The values of the bind energies for Sb 3d doublets are in agreement with the reports of other research groups in the literature [70-76]. It is a common knowledge that the surface adsorbed oxygen 1s peak mostly overlaps with the Sb3 $d_{5/2}$  peak at binding energies between 529 and 530 eV [51, 72-76]. However in this report, it is envisaged that the tartaric acid complex in the solution triggered an environment that is conducive for rich sulphide group and thus inhibits the formation of the oxide layer. The core-level spectra of the S 2p state give binding energies of 161.2 eV at the different deposition times, independent of the substrates as indicated in Figure 4b. It is generally understood that binding energy of the S<sup>2-</sup>-Sn<sup>2+</sup> bonding is an indication of single-phase SnS while the S<sup>2-</sup>-Sb<sup>3+</sup> are typical of S-Sb bonding structure in metallic sulfides. A typical combination of both bonding structures  $(S^{2-}-Sn^{2+}$  and  $S^{2-}-Sb^{3+})$  confirms the existence of single-phase Sn<sub>2</sub>Sb<sub>2</sub>S<sub>5</sub> thin films as obtained in this study and in line with the XRD plots as typified in Figures 1 and 2, respectively.

#### 3.4 Optical spectroscopy analysis

Figure 5 show the variation of the transmittance (T) in percentage (%) as function of the wavelength ( $\lambda$ ) in the range 300 to 1500 nm for films grown on SLG substrates. The transmittances were influenced by the different deposition times in that the higher values were recorded for films grown at the least deposition time. This behaviour is in line with variation in the film thickness, which increased with the deposition time up to 2h and decreased thereafter. This decreasing behaviour of film thickness with the corresponding change in transmittance was attributed to the effect of dissociation due to the longer deposition times. Variation in transmittance caused by varying deposition conditions including deposition time, film thickness, complexing agents, or other associated effects have been reported by other authors [1, 3, 20-21, 24, 32-33].

Data obtained from the transmittance and reflectance measurements were used to evaluate the following optical constants: (i) optical absorption coefficient ( $\alpha$ ), (ii) energy band gap (Eg), (iii) extinction coefficient (k), (iv) refractive index (n), and (v) dielectric constants ( $\varepsilon$ ). Appropriate equations from the literature [23–24, 40–48, 77] that were used for the analysis are as follows:

$$\alpha = \frac{1}{t} \ln \left( \frac{(1-R)^2}{T} \right) \tag{13}$$

$$(\alpha h \nu)^{x} = B(h \nu - E_{\sigma}) \tag{14}$$

$$n = \frac{\left(1 + \sqrt{R}\right)}{\left(1 - \sqrt{R}\right)} \tag{15}$$

$$k = \frac{\alpha \lambda}{4\pi} \tag{16}$$

$$\varepsilon = (n + ik)^2 = \varepsilon_i + \varepsilon_r \tag{17}$$

As indicated in Equations (13) and (14);  $\alpha$ , T, and t retain their meanings, R is the reflectance in percentage, h is the Planck's constant (6.64 × 10<sup>34</sup>Js),  $\nu$  is the frequency of the incident radiation, Eg is the energy bandgap, "x" is an index that determines the nature of the optical transition, and B is an energy independent constant that depends on the effective mass of the holes and electrons and refractive index of the material [77]. From Equations (15)–(17);  $\alpha$ ,  $\lambda$ , n, k, and  $\varepsilon$  retains their meanings, R is the reflectance,  $4\pi$  is a constant,  $\varepsilon_i$  and  $\varepsilon_r$  are the imaginary and real parts of the dielectric constants, respectively. The films displayed very high optical absorption coefficient in the respective

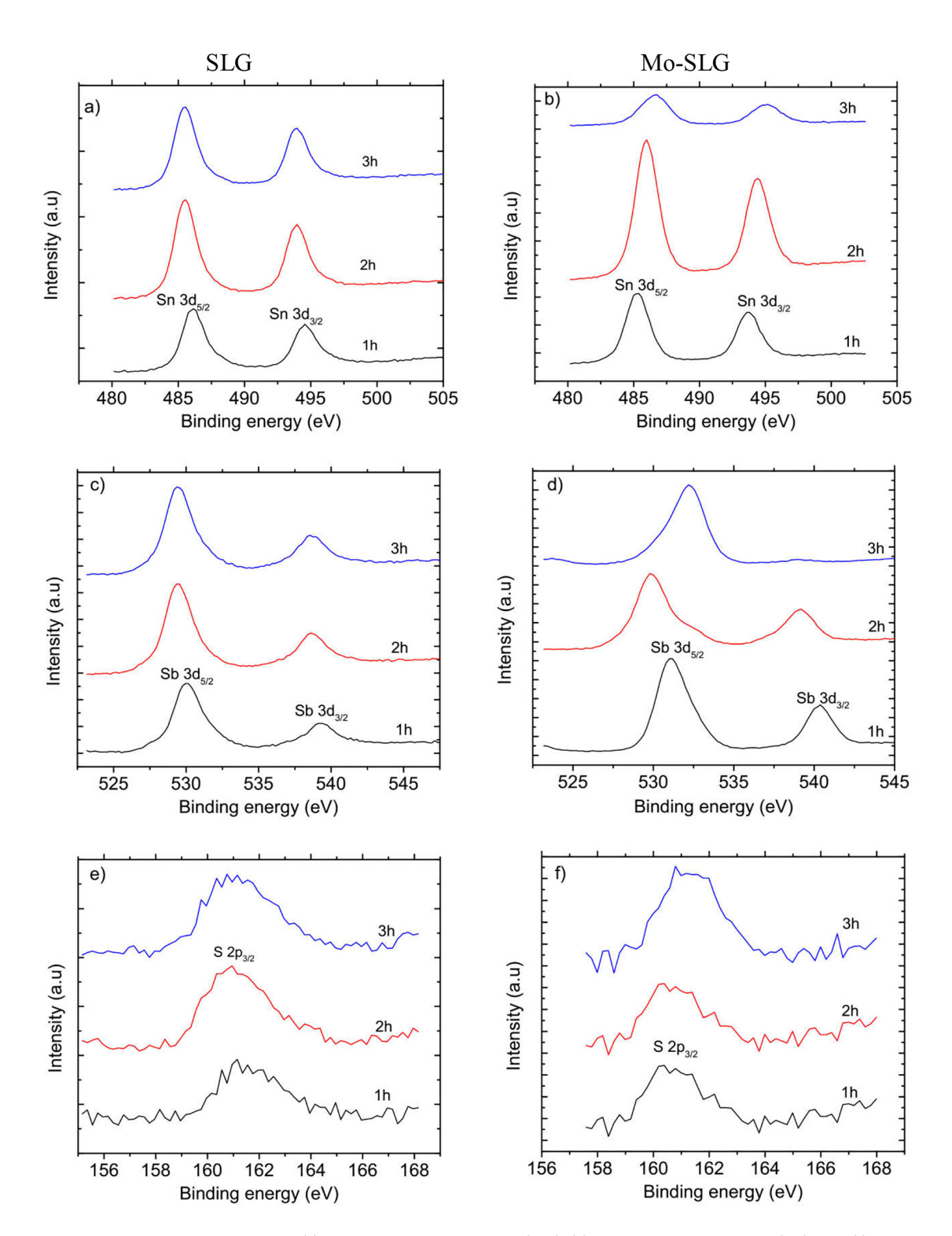


Figure 4b: XPS core-level spectra of; (a) Sn peaks on soda lime glass (SLG), (b) Sn peaks on molybdenum (Mo)-SLG, (c) Sb peaks on SLG, (d) Sb peaks on Mo-SLG, (e) S peaks on SLG, and (f) S peaks on Mo-SLG Sn<sub>2</sub>Sb<sub>2</sub>S<sub>5</sub> thin films at different deposition times.

deposition times. Thin films with optical absorption coefficient >10<sup>4</sup> cm<sup>-1</sup> are generally preferred for use as absorber layer in thin film heterojunction solar cells because such conditions enhance photocurrent generation. The energy band gaps were obtained using the plots of Equation (14) through extrapolation of the straight portion of the  $(\alpha h v)^2$ versus hv plots down the intercept on the photon energy (hv) axis. Values of the index "x" in Equation (14) are; 2 for

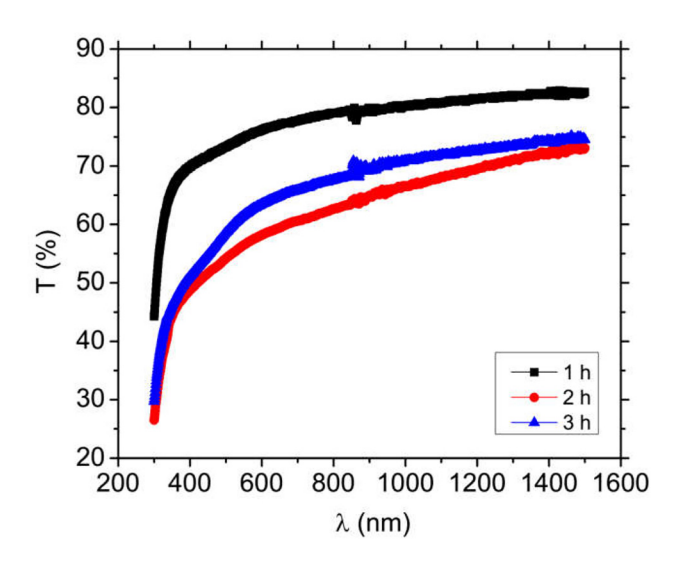
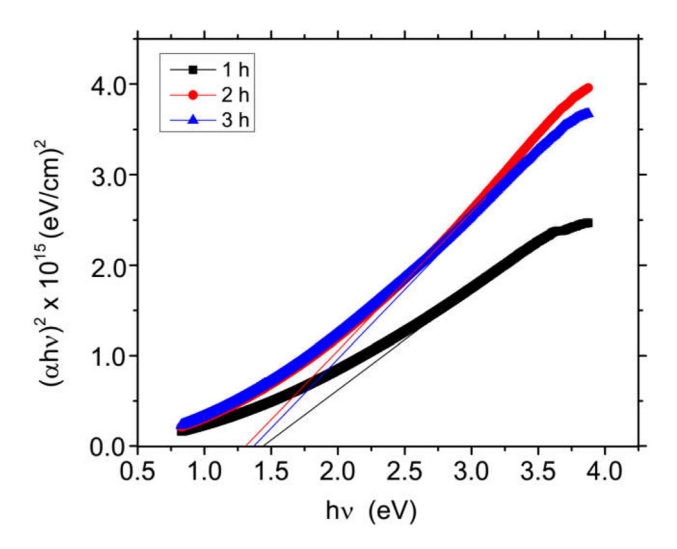


Figure 5: Transmittance (T) versus wavelength ( $\lambda$ ) plots of  $Sn_2Sb_2S_5$  thin films grown on soda lime glass (SLG) substrates.



**Figure 6:**  $(\alpha hv)^2$  versus hv plots of  $Sn_2Sb_2S_5$  thin films grown on soda lime glass (SLG) substrates.

direct energy bandgap, 0.5 for direct forbidden transition, and 1.5 for indirect forbidden transitions. Figure 6 show the graphs of  $(\alpha h v)^2$  versus h v for films grown at the respective deposition times on the SLG substrates.

The results give typical direct energy bandgap that varied with the deposition conditions. The energy bandgap was between 1.30 and 1.48 eV. The values of the energy bandgap exhibited the classic "bandgap narrowing effect" with respect to the growth conditions. This is due to quantum confinement arising from the improvement in the crystallinity of the films. The values of the energy bandgap are within the range reported by other research groups in  $(SnS)_x(Sb_2S_3)_y$  ( $1 \le x \le 5$ ,  $1 \le y \le 3$ ) thin films in the literature

**Table 5:** Variation of the optical constants of Sn<sub>2</sub>Sb<sub>2</sub>S<sub>5</sub> thin films grown on soda lime glass (SLG) substrates.

Deposition time (h)			Optical o	onstants
	Eg (eV)	n	k	ε
1	1.48	2.59	1.14	12.24
2	1.30	3.73	0.978	20.27
3	1.32	2.75	1.02	11.38

[1, 19–20, 76, 78–79]. Table 5 shows the variation of the optical constants  $(n, k, \text{ and } \varepsilon)$ , with the deposition conditions for films grown on the SLG substrates. The refractive index increased with the deposition time up to 2 h and decreased marginally. This behaviour is in line with the values of the film thickness at the respective deposition times. It is a common knowledge that the refractive index indicates how fast light travels through a medium and is usually defined by the relation  $n = c_v$ , where n and v retains their meanings and c is the speed of light in vacuum. The least value of the refractive index corresponded to the deposition time at which the films exhibited maximum film thickness as indicated in Table 4. This implies that the observation of the refractive indices shown on Table 5 is in agreement with the theory. The values of the refractive indices obtained in this study are very close to the report of other authors [22–23, 30, 79–80]. The extinction coefficient depends strongly on the absorption coefficient and the wavelength of the incident radiation. The values of the extinction coefficient exhibited marginal variation for deposition time ≤2 h, and increased thereafter. The dielectric constant was between 11.38 and 20.27. The variation of the dielectric constants also follows similar trend with the film thickness at the respective deposition times. High values of the dielectric constants are strong indicator for applications of the films in devices with high capacitance requirements and related optoelectronic devices. The values of the dielectric constants presented in this report are within the range reported by other authors in  $(SnS)_x(Sb_2S_3)_y$  (1  $\leq x \leq 5$ , 1  $\leq y \leq 3$ ) based thin films in the literature [7, 22, 24].

#### 3.5 Electrical studies

The summary of the electrical properties of the films grown on SLG substrates are shown in Table 6. The electrical resistivity of the films was between  $10^3$  to  $10^4$   $\Omega$ cm. The value of the electrical resistivity was least for films grown at a deposition time of 2 h. This correlates with the observation

p

3

Deposition time (h)				Electrical properties
	ρ (Ωcm)	p (cm <sup>-3</sup> )	μ (cm²/Vs)	Conductivity type
1	4.33 × 10 <sup>4</sup>	5.66 × 10 <sup>12</sup>	$2.55 \times 10^{1}$	р
2	$2.19\times10^3$	$6.01\times10^{12}$	$4.74\times10^{1}$	р

 $\boldsymbol{8.76\times10^{12}}$ 

Table 6: Variation of the electrical properties of the Sn<sub>2</sub>Sb<sub>2</sub>S<sub>5</sub> thin films grown on soda lime glass (SLG) substrates.

in the structural analysis as the films exhibited better crystallites size at that deposition condition. This will enhance increased flow of electrons due to the overall decreased grain boundary potential and thus leads to reduced electrical resistivity. The electrical resistivities obtained in this work are within the range reported by other authors in the literature [33, 36]. The carrier concentration was observed to be of the order of  $10^{12}$  cm<sup>-3</sup> while the hole mobilities varied from 21.5 to 47.4 cm<sup>2</sup>/Vs. The films exhibited p-type electrical conductivity at the respective deposition conditions. This observation is in agreement with the Sn-rich behaviour exhibited by the films as indicated in the compositional analysis. The Sn-rich  $Sn_2Sb_2S_5$  films will promote excess tin vacancies which are favourable conditions for p-conductivity behaviour.

 $3.31 \times 10^{4}$ 

#### 3.6 Photovoltaic properties

The photovoltaic properties of the  $\rm Sn_2Sb_2S_5$  thin films was explored by fabricating a glass/Mo/ $\rm Sn_2Sb_2S_5$ /CdS/i-ZnO/Al:ZnO/Ni/Al thin film heterojunction solar cell in the substrate configuration. Table 7 show the summary of the solar cell device parameters, including short-circuit current density ( $\rm J_{sc}$ ), open-circuit voltage ( $\rm V_{oc}$ ), fill-factor (FF), and the solar conversion efficiency ( $\eta$ ). The plots for the variation of the short-circuit current density with open-circuit voltage is shown on Figure 7. The results for the best device gave appreciable  $\rm J_{sc}$  of 20.02 mA/cm²,  $\rm V_{oc}$  of 0.012 V,

**Table 7:** Solar cell device properties of the  $Sn_2Sb_2S_5$ -based thin film solar cells as a function of deposition time.

Deposition time (h)			Device pro	perties
	Voc (V)	Jsc (mA cm <sup>-2</sup> )	FF (%)	η (%)
1	0.015	3.93	0.22	0.01
2	0.012	20.02	0.16	0.04
3	0.013	7.85	0.17	0.02

and a solar conversion efficiency of 0.04%. Although the solar conversion efficiency was generally low, the lower values obtained from devices made with Sn<sub>2</sub>Sb<sub>2</sub>S<sub>5</sub> absorber layers grown at deposition times of 1 and 3 h was possibly due to the relatively smaller crystallites sizes of the Sn<sub>2</sub>Sb<sub>2</sub>S<sub>5</sub> absorber layers at those deposition conditions as indicated in Table 3. This will introduce significant recombination and low diffusion length of charge carriers and consequently reduce the short-circuit current density as observed in Table 7. Reports of other research groups [49, 51, 54] in  $(SnS)_x(Sb_2S_3)_y$  (1  $\le x \le 5$ , 1  $\le y \le 3$ )-based thin film solar cells shown on Table 8, yielded higher opencircuit voltage values but higher short-circuit current densities were recorded in the present investigation. This was possibly due to the different phases of the  $(SnS)_x(Sb_2S_3)_y$  (1  $\leq x \leq 5$ , 1  $\leq y \leq 3$ ) absorber layers as indicated in Table 8. Generally the low solar conversion efficiency was attributed to a variety of factors including: (i) The Sn<sub>2</sub>Sb<sub>2</sub>S<sub>5</sub> absorber layer being a ternary compound is bound to have considerable lattice mismatch during film formation. This will contribute in no small measure to increased recombination effect across the junction, and

 $2.15 \times 10^{1}$ 

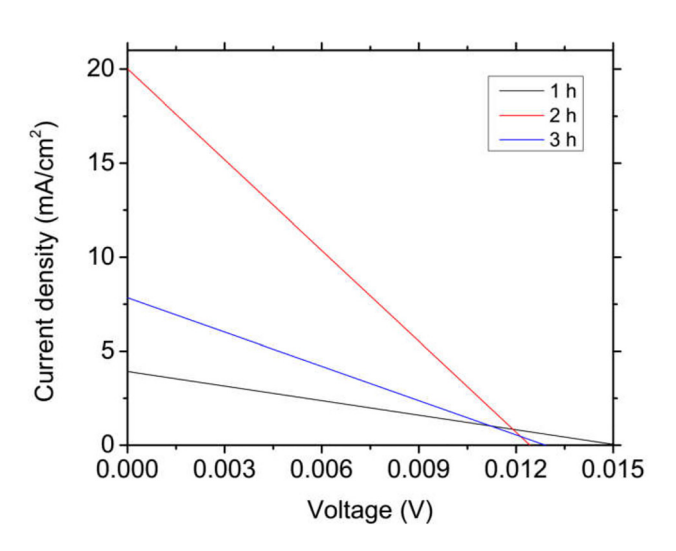


Figure 7: Current density-voltage (J-V) plots of  $\rm Sn_2Sb_2S_5$ -based thin film solar cells.

**Table 8:** Literature of  $(SnS)_x(Sb_2S_3)_y$   $(1 \le x \le 5, 1 \le y \le 3)$ -based thin film solar cells to date.

References	Device pro	Absorber			
	Voc (V)	Jsc (mA cm <sup>-2</sup> )	FF (%)	η (%)	layer
[49]	0.448	2.4	Not given	Not given	SnSb <sub>2</sub> S <sub>4</sub>
[51]	0.409	1.46	0.25	Not given	$Sn_6Sb_{10}S_{21}$
[54]	Not given	16.82	Not given	Not given	$Sn_3Sb_2S_6$
[This work]	0.015	3.93	0.22	0.01	$Sn_2Sb_2S_5$
[This work]	0.012	20.02	0.16	0.04	$Sn_2Sb_2S_5$
[This work]	0.013	7.85	0.17	0.02	$Sn_2Sb_2S_5$

thus reduce the solar conversion efficiency. (ii) Mismatch of band alignment between the interface of the Sn<sub>2</sub>Sb<sub>2</sub>S<sub>5</sub> absorber layer and the CdS window partner. Although band alignment investigation was not done in this work, it remains a clear possibility. (iii) Lastly, losses arising from series and parallel resistances contribute significant power loss in the device. Sn<sub>2</sub>Sb<sub>2</sub>S<sub>5</sub>-related thin film solar cell devices is novel, hence further research to investigate such power loss is a step in the right direction.

#### 4 Conclusions

Sn<sub>2</sub>Sb<sub>2</sub>S<sub>5</sub> thin films were successfully grown on SLG and Mo-SLG substrates using the CBD method. The structural, morphological, compositional, optical, electrical, and device properties were investigated with respect to the deposition conditions. Structural and compositional analysis showed that the films exhibit single phase at the respective deposition conditions. Optical studies give optical absorption coefficient >10<sup>4</sup> cm<sup>-1</sup>, and direct energy bandgap in the range suitable for optoelectronic application including thin film solar cell devices. Hall effect measurements indicated that the deposited Sn<sub>2</sub>Sb<sub>2</sub>S<sub>5</sub> films possess p-type electrical conductivity. The photovoltaic properties of the Sn<sub>2</sub>Sb<sub>2</sub>S<sub>5</sub>-related thin film solar cells give a short-circuit current density of 20 mA/cm<sup>2</sup> with solar conversion efficiency of 0.04% for the best device.

**Acknowledgments:** Dr. P.A. Nwofe is grateful to Matsuame International Foundation (MIF), Japan for the award of Post-doctoral Research Fellowship; Sugiyama Laboratory, Tokyo University of Science Japan for host; and Ebonyi

State University, Abakaliki, Nigeria for approval of study leave. The authors also acknowledge the contributions of T. Tosuke, A. Kanai, and T. Funatsu in the XPS and SEM measurements, Dr. I. Khatri and Dr. I. Kim for useful discussions.

**Author contribution:** All the authors have accepted responsibility for the entire content of this submitted manuscript and approved submission.

Research funding: None declared.

Conflict of interest statement: The authors declare no conflicts of interest regarding this article.

#### References

- [1] N. Khedmi, M. Ben Rabeh, F. Asougi, and M. Kanzari, "Effect of vacuum annealing on structural, morphological and optical properties of Sn<sub>2</sub>Sb<sub>2</sub>S<sub>5</sub> thin films with different thicknesses", Eur. Phys. J. Appl. Phys., vol. 69, 2015, Art no. 10303.
- [2] M. Ben Rabeh, N. Khedmi, and M. Kanzari, "Prospect for SnmSb2nS3n+m(n = 1, m = 1, 2, 3) sulfosalt compounds", J. Mater. Sci. Mater. Electron., vol. 26, pp. 2002-2009, 2015.
- [3] D. Abdelkader, A. Jebali, A. Larbi, A. Harizi, and M. Kanzari, "Synthesis, characterization, structural and optical absorption behavior of SnxSbySz powders", Adv. Powder Technol., vol. 27, pp. 734-741, 2016.
- [4] D. Abdelkader, M. Ben Rabeh, Khedmi, and M. Kanzari, "Investigation on optical properties of SnxSbySz sulfosalts thin films", Mater. Sci. Semicon. Proc., vol. 21, pp. 14-19, 2014.
- [5] I. Gaied, A. Gassoumi, M. Kanzari, and N. Yacoubi, "Investigation of optical properties of the sulfosalt new absorber Sn<sub>2</sub>Sb<sub>2</sub>S<sub>5</sub> thin films using photo-thermal defection spectroscopy", J. Phys. Conf. Ser., vol. 214, 2010, Art no. 012127.
- [6] A. Mami, M. A. Wederni, N. Bennaji, et al., "Investigation of the thermal annealing effect on the optical, thermal and electrical properties of Sn<sub>2</sub>Sb<sub>2</sub>S<sub>5</sub> evaporated thin films", Opt. Quant. Elect., vol. 52, pp. 1-17, 2020.
- [7] Y. Fadhil, A. Rabhi, and M. Kanzari, "Determination and analysis of optical constant of annealed Sn<sub>2</sub>Sb<sub>2</sub>S<sub>5</sub> thin films", Acta Metall. Sin., vol. 28, pp. 656-662, 2015.
- [8] A. Gassoumi, and M. Kanzari, "Sn<sub>2</sub>Sb<sub>2</sub>S<sub>5</sub> films for photovoltaic applications", J. Optoelect. Adv. Mater., vol. 11, pp. 414-420, 2009.
- [9] A. Gassoumi, M. Kanzari, and B. Rezig, "The effect of substrate temperature on the properties of the sulfosalt Sn<sub>2</sub>Sb<sub>2</sub>S<sub>5</sub> thin film", Sensor Letts., vol. 9, pp. 2376-2379, 2011.
- [10] A. Gassoumi, and M. Kanzari, "Optical, structural and electrical properties of the new absorber Sn<sub>2</sub>Sb<sub>2</sub>S<sub>5</sub> thin flms", Chalcogenide Lett., vol. 6, pp. 163-170, 2009.
- [11] N. Khedmi, D.M BenRabehAbdelkadher, F. Ousgi, and M. Kanzari, "Effect of thickness on structural and optical properties of vacuum-deposited Sn<sub>2</sub>Sb<sub>2</sub>S<sub>5</sub> thin films Cryst", Res. Technol., pp. 1-8, 2014.
- [12] N. Ali, A. Hussain, S. T. Hussain, et al., "Physical properties of the absorber layer Sn<sub>2</sub>Sb<sub>2</sub>S<sub>5</sub> thin films for photovoltaics", Curr. Nanosci., vol. 9, pp. 149-152, 2013.

- [13] N. Ali, R. Ahmed, B. Haq, A. Shaari, R. Hussain, and S. Goumri-Said, "A novel approach for the synthesis of tin antimony sulphide thin films for photovoltaic applications", Sol. Energy, vol. 113, pp. 25-33, 2015.
- [14] D. Abdelkader, F. C. Akkari, Khedmi, B. Gallas, F. Antoni, and M. Kanzari, "Structural and spectroscopic ellipsometry studies on vacuum-evaporated  $Sn_{2m-4}Sb_4S_{2m+2}$  (m = 2.5, 3 and 4) thin films deposited on glass and Si substrates", J. Alloys Compd., vol. 646, pp. 1049-1057, 2015.
- [15] M. A. Khan, A. Ahmed, N. Ali, et al., "Improved optical properties of tin antimony sulphide thin films for photovoltaics," Am. J. Mater. Sci. Eng., vol. 4, pp. 1-6, 2016.
- [16] N. Ali, S. Ajmal, M. Shah, R. Ahmed, and B. A. Shaari, "Effect of antimony variation on the physical properties of SnSbS thin films," Chalcogenide Lett., vol. 11, pp. 503-508, 2014.
- [17] Y. Fadhil, A. Rabhi, and M. Kanzari, "Annealing effects on the physical properties of thermally evaporated Sn<sub>2</sub>Sb<sub>2</sub>S<sub>5</sub> thin films", in IEEE First International Conference on Green Energy (ICGE), Sfax, Tunisia, IEEE, pp. 124-128, 2014.
- [18] I. Mellouki, A. Mami, N. Bennaji, and Y. Fadhli, "Study of doping and annealing effects on thermal properties of  $Sn_xSb_2S_v$  (1  $\leq x \leq$ 3, 4≤ y≤ 6) sulfosalts thin films by electro-pyroelectric technique", Thermochim. Acta, vol. 670, pp. 123-127, 2018.
- [19] N. Ali, R. Ahmed, A. Shaari, B.-U. Haq, N. Ahmad, and S. M. Abbas, "Synthesis and characterization of Sn-Sb-S thin films for solar cell applications by sputtering techniques", Kovove Mater., vol. 52, pp. 219-223, 2014.
- [20] A. Gassoumi, and M. Kanzari, "Growth and post-annealing effect on the properties of the new sulfosalt SnSb<sub>2</sub>S<sub>4</sub> thin film", Phys. E, vol. 44, pp. 71-74, 2011.
- [21] A. Gassoumi, M. Kanzaria, and B. Rezig, "Thermally induced changes in optical and electrical properties of SnSb<sub>2</sub>S<sub>4</sub> thin films", Eur. Phys. J. Appl. Phys., vol. 41, pp. 91-95, 2008.
- [22] Y. Fadhil, A. Rabhi, and M. Kanzari, "Effect of air annealing on dispersive optical constants and electrical properties of SnSb<sub>2</sub>S<sub>4</sub> thin films", Mater. Sci. Semicon. Proc., vol. 26, pp. 282-287, 2014.
- [23] N. R. Ali, S. T. Hussain, Y. Khan, N. Ahmad, M. A. Igbal, and S. M. Abbas, "Effect of air annealing on the band gap and optical properties of SnSb<sub>2</sub>S<sub>4</sub> thin films for solar cell application", Mater. Lett., vol. 100, pp. 148-151, 2013.
- [24] I. M. El Radaf, "Dispersion parameters, linear and nonlinear optical analysis of the SnSb<sub>2</sub>S<sub>4</sub> thin films", Appl. Phys. A, vol. 126, pp. 357, 2020.
- [25] M. Ben Rabeh, N. Khedmi, and M. Kanzari, "Vacuum annealing effects on the structural and optical properties of SnSb<sub>2</sub>S<sub>4</sub> thin films fabricated by thermal evaporation technique", Optik, vol. 126, pp. 3104-3109, 2014.
- [26] A. Larbi, I. Trabelsi, H. Dahman, and M. Kanzari, "Investigation on the AC and DC electrical conductivity of Sn<sub>3</sub>Sb<sub>2</sub>S<sub>6</sub> thin films prepared by glancing angle deposition," J. Mater. Sci. Mater. Elect., vol. 29, pp. 2907-2914, 2018.
- [27] N. Khedmi, M. Ben Rabeh, and M. Kanzari, "Structural, morphological and optical properties of SnSb<sub>2</sub>S<sub>4</sub> thin films grown by vacuum evaporation method", J. Mater. Sci. Tech., vol. 30, pp. 1006-1011, 2014.
- [28] N. Ali, S. T. Hussain, M. A. Igbal, K. Hutching, and D. Lane, "Structural and optoelectronic properties of antimony tin sulphide thin films deposited by thermal evaporation techniques", Optik, vol. 124, pp. 4746-4749, 2013.

- [29] A. Nisar, R. Ahmed, A. Shaari, et al., "Annealing effects on the structural and optical properties of thermally deposited tin antimony sulfide thin films", Braz. J. Phys., vol. 44, pp. 733-738, 2014.
- [30] A. Jebali, N. Khedmi, and M. Kanzari, "The effect of annealing in N<sub>2</sub> atmosphere on the physical properties of SnSb<sub>4</sub>S<sub>7</sub> thin films", J. Alloys Compd., vol. 673, pp. 38-46, 2016.
- [31] A. Jebali, M. Ben Rabeh, N. Khemiri, and M. Kanzari, "The effect of substrate temperature on the optical properties of SnSb<sub>4</sub>S<sub>7</sub> thin films", Mater. Res. Bull., vol. 61, pp. 363-368,
- [32] A. Jebali, N. Khedmi, F. Aousgi, M. Ben Rabeh, and M. Kanzari, "Structural, morphological and optical properties of the sulfosalt material SnSb<sub>4</sub>S<sub>7</sub> thin films", Mater. Sci. Semicon. Proc., vol. 27, pp. 1057-1064, 2014.
- [33] T. Imen, A. Jebali, and M. Kanzari, "Electrical characterization of SnSb<sub>4</sub>S<sub>7</sub> thin films by impedance spectroscopy", J. Mater. Sci. Mater. Electron., vol. 27, pp. 4326-4335, 2016.
- [34] N. Drissi, A. Gassoumi, H. Boughzala, J. Ouerfelli, and M. Kanzari, "Investigation of structural and optical properties of the sulfosalt SnSb<sub>4</sub>S<sub>7</sub> thin films", J. Mol. Struct., vol. 1047, pp. 61-65, 2013.
- [35] N. D. Khedmi, A. Abdelkader, F. Jebali, and M. Kanzari, "Effects of excimer laser annealing energy on the properties of thermally evaporated tin antimony sulfide thin films and TEM characterization of the powder", J. Mater. Sci. Mater. Electron., vol. 29, pp. 16295-16304, 2018.
- [36] N. Ali, A. Hussain, R. Ahmed, W. N. Wan Shamsuri, N. M. Abdel-Salam, and R. Khenata, "Fabrication and characterization of 150 nm tin antimony sulfide thin films, a promising window layer material for homojunction solar cells", Appl. Phys. A, vol. 123, pp. 282, 2017.
- [37] A. Harizi, M. Ben Rabeh, F. Laatar, F. Chaffar Akkari, and M. Kanzari, "Substrate temperature dependence of structural, morphological and optical properties of Sn<sub>4</sub>Sb<sub>6</sub>S<sub>13</sub> thin films deposited by vacuum thermal evaporation", Mater. Res. Bull., vol. 79, pp. 52-62, 2016.
- [38] A. Harizi, A. Sinaoui, F. Chaffar Akkari, and M. Kanzari, "Physical properties of Sn<sub>4</sub>Sb<sub>6</sub>S<sub>13</sub> thin films prepared by a glancing angle deposition method", Mater. Sci. Semicond. Proc., vol. 41, pp. 450-456, 2016.
- [39] A. Harizi, M. Ben Rabeh, and M. Kanzari, "Substrate temperature-dependent physical properties of thermally evaporated  $Sn_4Sb_6S_{13}$  thin films", Acta Metall. Sin., vol. 29, pp. 79-88, 2016.
- [40] A. Larbi, N. Khedmi, and M. Kanzari, "The effect of the growth condition on the properties of the new material Sn<sub>3</sub>Sb<sub>2</sub>S<sub>6</sub> thin films", Int. J. Thin Films Sci. Tech., vol. 3, pp. 27-34, 2014.
- [41] D. Abdelkader, F. Chaffar Akkari, N. Khemiri, et al., "Effect of SnS addition on the morphological and optical properties of (SnS)m (Sb<sub>2</sub>S<sub>3</sub>)n nano-rods elaborated by glancing angle deposition", Phys. B Condens. Matter, vol. 546, pp. 33-43, 2018.
- [42] P. P. K. Smith, "Structure determination of diantimony tritinhexasulphide, Sn<sub>3</sub>Sb<sub>2</sub>S<sub>6</sub> by high resolution transmission electron microscopy", Acta Cryst. Sect. C Cryst. Struct., vol. 40, pp. 581-584, 1984.
- [43] A. Nisar, R. Ahmed, H. Bakhtiar ul, A. Shaari, and M. Jabeen, "200° C annealed combinatorially deposited chalcogenide based metallic thin films for photovoltaics", Measurement, vol. 63, pp. 81-86, 2015.

- [44] N. Mehrez, N. Ben, N. Khedmi, and M. Kanzari, "Study of structural and morphological properties of thermally evaporated Sn<sub>2</sub>Sb<sub>6</sub>S<sub>11</sub> thin films", Mater. Chem. Phys., vol. 182, pp. 133-138, 2016.
- [45] A. Harizi, "Microstructural and optical properties of Sn<sub>4</sub>Sb<sub>6</sub>S<sub>13</sub> nanocrystals deposited on PAA templates", Mater. Res. Bull., vol. 125, 2020, Art no. 10791.
- [46] I. Trabelsi, A. Harizi, and M. Kanzari, "Complex impedance spectroscopy of Sn<sub>4</sub>Sb<sub>6</sub>S<sub>13</sub> thin films deposited by thermal vacuum evaporation", Thin Solid Films, vol. 631, pp. 161-171, 2017.
- [47] N. Bennaji, R. Lahouli, Y. Fadhil, and I. Mellouki, "Tuning of the electrical and thermal properties of SnSb<sub>2</sub>S<sub>4</sub> sulfosat vacuum evaporated thin films subjected to a heat treatment for thermoelectric applications", Sensor. Actuator., vol. 282, pp. 67-75, 2018.
- [48] A. Larbi, F. Chaffar Akkari, H. Dahman, D. Demaille, B. Gallas, and M. Kanzari, "Structural, morphological and optical properties of Sn<sub>3</sub>Sb<sub>2</sub>S<sub>6</sub> thin films synthesized by oblique angle deposition", J. Electron. Mater., vol. 45, pp. 5487-5496, 2016.
- [49] L. A. Rodríguez-Guadarrama, I. L. Alonso-Lemus, J. Campos-Álvarez, and J. Escorcia-García, "Novel SnSb<sub>2</sub>S<sub>4</sub> thin films obtained by chemical bath deposition using tartaric acid as complexing agent for their application as absorber in solar cells", MRS Adv., vol. 4, pp. 2035-2042, 2019.
- [50] S. Mushtaq, B. Ismail, M. Aurang Zeb, N. J. Suthan Kissinger, and A. Zeb, "Low-temperature synthesis and characterization of Sndoped Sb<sub>2</sub>S<sub>3</sub> thin film for solar cell applications", J. Alloys Compd., vol. 632, pp. 723-728, 2015.
- [51] S. Devasia, S. Shaji, D. A. Avellaneda, J. A. Martinez, and B. Krishnan, "Tin antimony sulfide (Sn<sub>6</sub>Sb<sub>10</sub>S<sub>21</sub>) thin films by heating chemically deposited Sb<sub>2</sub>S<sub>3</sub>/SnS layers: studies on the structure and their optoelectronic properties", J. Alloys Compd., vol. 827, 2020, Art no. 154256.
- [52] U. Chalapathi, B. Poornaprakash, A. Chang-Hoi, and P. Si-Hyun, "Large-grained Sb<sub>2</sub>S<sub>3</sub> thin films with Sn-doping by chemical bath deposition for planar heterojunction solar cells", Mater. Sci. Semicon. Proc., vol. 84, pp. 138-143, 2018.
- [53] P. A. Nwofe, and M. Sugiyama, "Microstructural, optical, and electrical properties of chemically deposited tin antimony sulfide thin films for use in optoelectronic devices", *Phys. Status* Solidi, 2020, Art no. 1900881. https://doi.org/10.1002/pssa. 201900881.
- [54] E. Barrios-salgado, Y. Rodriguez-Lacano, J. P. Perez-orozoco, and A. R. Garcia-Angelmo, "A new route for synthesis of Sn<sub>2</sub>Sb<sub>3</sub>S<sub>6</sub> thin films by chemical deposition", Revista Mexicana De Ingineria Quimica, vol. 19, pp. 1363-1373, 2020.
- [55] S. N. Mark, E. W. Singh, and J. McFarlandBaltrusaitis, "Electrochemically deposited Sb and in doped tin sulfide (SnS) photoelectrodes", J. Phys. Chem. C, vol. 119, pp. 6471-6480, 2015.
- [56] F. Tlig, M. Gannouni, I. Ben Assaker, and R. Chtourou, "New investigation on the physical and electrochemical properties of (TAS) thin films grown by electro-deposition technique", J. Photochem. Photobiol. A, vol. 335, pp. 26-35, 2017.
- [57] W. Kumrueng, K. Sawanthai, A. Tubtimtae, and W. Ponhan, "Effect of pH treatment on the structural and optical properties of Sn<sub>6</sub>Sb<sub>10</sub>S<sub>21</sub> thin films faciley synthesized using a spin coating method", Opt. Mater., vol. 105, 2020, Art no. 109917.
- [58] J. C. Jumas, J. Olivier-Fourcade, E. Philippot, and M. Maurin, "Sur le système Sn-Sb-S: étude structurale du composé sulfuré mixte d'étain (II et IV) et d'antimoine (III) Sn<sub>5</sub>Sb<sub>2</sub>S<sub>9</sub>", Rev. Chim. Miner., vol. 16, pp. 48-59, 1979.

- [59] J. C. Jumas, J. Olivier-Fourcade, E. Philippot, and M. Maurin, "Sur le système SnS-Sb<sub>2</sub>S<sub>3</sub>étude structurale de Sn<sub>4</sub>Sb<sub>6</sub>S<sub>13</sub>", Acta Crystallogr., vol. B36, pp. 2940-2945, 1980.
- [60] J. B. Parise, P. P. K. Smith, and C. J. Howard, "Crystal structure refinement of Sn<sub>3</sub>Sb<sub>2</sub>S<sub>6</sub> by high-resolution neutron powder diffraction", Mater. Res. Bull., vol. 19, pp. 503-508,
- [61] N. Bennaji, Y. Fadhil, I. Mellouki, et al., "Electrical and dielectric characteristics of SnSbS thin films for solar cell applications", J. Electron. Mater., vol. 49, pp. 1354-1361, 2020.
- [62] J. B. Parise, and P. P. K. Smith, "Structure of the tin antimony sulphide Sn<sub>6</sub>Sb<sub>10</sub>S<sub>21</sub>", Acta Crystallogr., vol. C40, pp. 1772-1776, 1984.
- [63] A. Gassoumi, H. Meradji, and N. Kamoun-Turki, "First principles study of electronic and optical properties of the ternary SnSb<sub>4</sub>S<sub>7</sub> using modified Becke-Johnson potential", Mater. Sci. Semicond. Proc., vol. 40, pp. 262-266, 2015.
- [64] N. WANG, and D. Eppelsheimer, "The ternary phases in the system Sn-Sb-S", Chem. Erde, vol. 35, pp. 179-184, 1976.
- [65] I. Grozdanov, "A simple and low-cost depoition for electrless deposition of chalcogenide thin films", Semicond. Sci. Technol., vol. 9, pp. 1234, 1994.
- [66] Joint Committee on Powder and Diffraction Standards (JCPDS) No. 00-044-0829.
- [67] P. A. Nwofe, K. T. Ramakrishna Reddy, G. Sreedevi, J. K. Tan, and R. W. Miles, "Structural, optical, and electro-optical properties of thermally evaporated tin sulphide layers", Jpn. J. Appl. Phys., vol. 51, 2012, Art no. 10NC36.
- [68] P. P. K. Smith, and B. G. Hyde, "The homologous series Sb<sub>2</sub>S and PbS: structures of diantimony dilead pentasulphide, Pb2Sb2S5, and the related phase diantimony ditin pentasulphide, Sn<sub>2</sub>Sb<sub>2</sub>S<sub>5</sub>", *Acta Cryst.*, vol. C39, pp. 1498–1502, 1983.
- [69] S. Gedi, V. R. M. Reddy, T. R. R. Kotte, Y. Park, and W. K. Kim, "Effect of C<sub>4</sub>H<sub>6</sub>O<sub>6</sub> concentration on the properties of SnS thin films for solar cell applications", Appl. Surf. Sci., vol. 465, pp. 802-815, 2019.
- [70] S. Shaji, L. V. Garcia, S. L. Loredo, et al., "Antimony sulfide thin films prepared by laser assisted chemical bath deposition", Appl. Surf. Sci., vol. 393, pp. 369-376, 2017.
- [71] R. G. Avilez Garcia, C. A. Meza Avendaño, M. Pal, F. Paraguay Delgado, and N. R Mathews, "Antimony sulfide (Sb<sub>2</sub>S<sub>3</sub>) thin films by pulse electrodeposition: effect of thermal treatment on structural, optical and electrical properties", Mater. Sci. Semicon. Proc., vol. 44, pp. 91-100, 2016.
- [72] M. Tamilselvan, A. Byregowda, C.-Y. Su, C.-J. Tseng, A. J. Bhattacharyya, Planar heterojunction solar cell employing a single-source precursor solution-processed Sb<sub>2</sub>S<sub>3</sub> thin film as the light absorber. ACS Omega vol. 4, pp. 11380-11387,
- [73] K. S. Swapnil, K. Banerjee, S. Majumder, and B. R. Sankapal, "Novel application of non-aqueous chemical bath deposited Sb<sub>2</sub>S<sub>3</sub> thin films as super-capacitive electrode", *Inter. J. Hydrog*. Energy, vol. 41, pp. 21278-21285, 2016.
- [74] R. Tang, X. Wang, C. Jiang, et al., n-Type doping of Sb<sub>2</sub>S<sub>3</sub> lightharvesting films enabling high-efficiency planar heterojunction solar cells. ACS Appl. Mater. Interfaces vol. 10, pp. 30314-30321,
- [75] V. P. Zakaznova-Herzog, S. L. Harmer, H. W. Nesbitt, G. M. Bancroft, R. Flemming, A. R. Pratt, High resolution XPS study of the large-band-gap semiconductor stibnite (Sb<sub>2</sub>S<sub>3</sub>):

- structural contributions and surface reconstruction. Surf. Sci. vol. 600, pp. 348-356, 2006.
- [76] A. Serin, S. Korkmaz, F. Meydaneri Tezel, and I. A. Kariper, "Synthesis of go: SnSbS thin films and the analysis of electrochemical performance", J. Alloys Compd., 2020, Art no. 154908. https://doi.org/10.1016/j.jallcom.2020. 154908.
- [77] J. I. Pankove, Optical Processes in Semiconductors, Englewood Cliffs, New Jersey, Prentice-Hall, 1971.
- [78] M. H. Behbahani, H. Fallah, and H. Esfandiary, "The thickness and deposition rate effects on structural and optical properties of aluminized PET", Appl. Phys. A, vol. 126, pp. 356, 2020.
- [79] N. S. Tezel, F. M. Tezel, and İ. A. Kariper, "Surface and electrooptical properties of amorphous Sb<sub>2</sub>S<sub>3</sub> thin films", Appl. Phys. A, vol. 125, pp. 198, 2019.
- [80] N. Ali, A. Hussain, R. Ahmed, et al., "Antimony sulphide, an absorber layer for solar cell application", Appl. Phys. A, vol. 122, pp. 23, 2016.